remote sensing

MDPI

Technical Note

Unraveling the Influence of Equatorial Waves on Post-Monsoon Sea Surface Salinity Anomalies in the Bay of Bengal

Shuling Chen [1,2], Fuwen Qiu [1,2,*], Chunsheng Jing [1,2], Yun Qiu [1,2,3,4] and Junpeng Zhang [1,2]

[1] The Third Institute of Oceanography, Ministry of Natural Resources, Xiamen 361005, China; chenshuling@tio.org.cn (S.C.); jingcs@tio.org.cn (C.J.); qiuyun@tio.org.cn (Y.Q.); zhangjunpeng@tio.org.cn (J.Z.)
[2] Fujian Provincial Key Laboratory of Physical and Geological Processes, Xiamen 361005, China
[3] Southern Marine Science and Engineering Guangdong Laboratory (Zhuhai), Zhuhai 519080, China
[4] Laboratory for Regional Oceanography and Numerical Modeling, Qingdao National Laboratory for Marine Science and Technology, Qingdao 266237, China
* Correspondence: qiufuwen@tio.org.cn

Abstract: In this study, we investigate the connection between planetary equatorial waves, modulated by the Indian Ocean dipole (IOD) and El Niño Southern Oscillation (ENSO), and the interannual variabilities of the salinity distribution in the Bay of Bengal (BoB) in October–December (OND), along with its associated dynamics, using satellite and reanalysis datasets. In OND 2010 and 2016 (1994, 1997, 2006, and 2019), positive (negative) sea surface salinity anomalies (SSSAs) were distributed in the eastern equatorial Indian Ocean (EIO) and Andaman Sea. Moreover, the southward movement of negative (positive) SSSAs along the eastern Indian coast was observed. This phenomenon was caused by large-scale anomalous currents associated with zonal wind over the EIO. During OND 2010 and 2016 (1994, 1997, 2006, and 2019), due to anomalous westerlies (easterlies) over the EIO and anomalous downwelling (upwelling) Kelvin waves, the strengthened (weakened) Wyrtki jet and the basin-scale anomalous cyclonic (anticyclonic) circulation in the BoB gave rise to positive (negative) SSSAs within the eastern EIO and Andaman Sea. In addition, the intensified (weakened) eastern Indian coastal currents led to the southward movement of negative (positive) SSSAs. It is worth noting that downwelling Kelvin waves reached the western coast of India during OND 2010 and 2016, while upwelling Kelvin waves were only confined to the eastern coast of India during OND 1994, 1997, 2006, and 2019. Furthermore, westward salinity signals associated with reflected westward Rossby waves could modulate the spatial pattern of salinity. The distribution of salinity anomalies could potentially influence the formation of the barrier layer, thereby impacting the sea surface temperature variability and local convection.

Keywords: Bay of Bengal; sea surface salinity; Kelvin waves; Rossby waves; Indian Ocean dipole; El Niño Southern Oscillation (ENSO)

check for updates

Citation: Chen, S.; Qiu, F.; Jing, C.; Qiu, Y.; Zhang, J. Unraveling the Influence of Equatorial Waves on Post-Monsoon Sea Surface Salinity Anomalies in the Bay of Bengal. *Remote Sens.* **2024**, *16*, 1348. https://doi.org/10.3390/rs16081348

Academic Editors: Antonio Pepe, Jiayi Pan, Fusun Balik Sanli and Qing Zhao

Received: 27 February 2024
Revised: 2 April 2024
Accepted: 8 April 2024
Published: 11 April 2024

1. Introduction

The Bay of Bengal (BoB) exhibits the lowest sea surface salinity (SSS) compared to other parts of the Indian Ocean due to its excess precipitation over evaporation and dramatically increased discharge from rivers [1,2]. Strong salinity stratification with a shallow mixed layer caused by a low SSS is conducive to the formation of a barrier layer, which may affect air–sea interactions [3–5].

The interannual variability of the salinity in the BoB is significant in boreal fall, especially in the northern BoB, the coastal region of east India and the Andaman Sea [6–9]. The interannual variability of the SSS in the northern BoB is primarily influenced by the discharge from the Ganga–Brahmaputra river runoff, while in the coastal region of eastern India and the Andaman Sea, it is predominantly driven by horizontal advection associated with the Indian Ocean dipole (IOD) and El Niño Southern Oscillation (ENSO).

Interannual variations in equatorial winds associated with the IOD and ENSO dominate the currents in the equatorial Indian Ocean (EIO), which could influence the interannual variations in the salinity distribution in the BoB [10]. After the summer monsoon, the zonal winds are mostly westerlies over the EIO, forming strong surface eastward currents, referred to as Wyrtki jets [11]. Wyrtki jets bifurcate into two branches and extend towards the BoB in the northern direction [12]. Easterly (westerly) equatorial wind anomalies associated with a negative IOD and La Niña (positive IOD and El Niño) induce stronger (weaker) Wyrtki jets, leading to an increased (decreased) intrusion of high-salinity water from the western EIO into the eastern BoB, which may increase (decrease) the salinity in both the eastern EIO and the eastern BoB [13].

Interannual variations in the equatorial winds associated with the IOD and ENSO could also modulate the circulation pattern in the BoB [1,14,15]. Forced by the semi-annual cycle of zonal wind in the EIO, in the local climatology, there are two pairs of upwelling Kelvin waves (the first one during January–March and the second one during August–September) and downwelling Kelvin waves (the first one during May–July and the second one during October–December, OND) evolving in the EIO and coastal BoB in each year [16]. Only the second downwelling Kelvin wave could reach the southeastern Arabian Sea, and it shows large interannual variability, caused primarily by variability in the equatorial westerly winds associated with the IOD and ENSO [16]. Due to the anomalous equatorial westerlies associated with a negative IOD and La Niña, strong coastal downwelling Kelvin waves manifest as a significantly positive sea level anomaly (SLA), found along the coast of the BoB, subsequently inducing basin-scale anomalous cyclonic circulation in the BoB [17,18]. Therefore, the intensity of the eastern Indian coastal current (EICC) in fall is enhanced during negative-IOD and La Niña years, resulting in more freshwater transported southward along the east coast of India. The opposite is true during positive-IOD and El Niño years [7,19].

The above discussion reveals that the zonal winds over the EIO associated with both the IOD and ENSO probably modulate the interannual variations in the salinity distribution in the BoB during the fall transition between the summer monsoon and winter monsoon. Thus, commencing with zonal wind over the EIO, in this study, we explore the contrast between salinity patterns against the background of different zonal winds and the impact of planetary equatorial waves activated by zonal wind on the salinity patterns. This paper is organized as follows: Section 2 describes the materials and methods we used in this study. Section 3 elucidates the linkage between zonal wind patterns in the EIO and the distribution of salinity anomalies in the BoB, along with its associated underlying mechanisms. The discussion is given in Section 4.

2. Materials and Methods

2.1. Materials

The hourly $0.25^\circ \times 0.25^\circ$ gridded zonal wind (U) at 10 m above the sea surface from the European Center for Medium-Range Weather Forecasts reanalysis V5 (ERA5) has been available since 1979 [20]. ERA5 is a reanalysis product from the European Center for Medium-Range Weather Forecasts (ECMWF) and can be downloaded from the Copernicus Climate Data Store. It is generated via data assimilation based on model data combined with global observations and measurements from satellites, radars, land stations, etc.

The Soil Moisture and Ocean Salinity (SMOS) version 8 Level 3 SSS product was obtained from the LOCEAN (Laboratoire d'Océanographie et du Climat: Expérimentations et Approches Numériques, Paris, France) expertise center of the CATDS (Centre Aval de Traitement des Données SMOS, Paris, France). The gridded SMOS SSS, smoothed with a 9-day Gaussian filter and with a 25 km median filter, covers the period of January 2010–December 2020 at 4-day intervals, with a spatial resolution of 25×25 km^2. The SMOS mission of the European Space Agency (ESA) was launched in November 2009 and has been continuously providing brightness temperature data in the L-Band since January 2010, which are used to retrieve soil moisture and SSS over the land and ocean, respectively. A previous study showed that the SMOS SSS compares well with in situ observations and other satellite products over the Bay of Bengal [7].

The daily averaged three-dimensional currents and salinity used for the analysis were obtained from the Copernicus Marine Environment Monitoring Service (CMEMS; http://marine.copernicus.eu, accessed on 23 March 2023; product ID: GLOBAL_MULTIYEAR_PHY_001_030; DOI: https://doi.org/10.48670/moi-00021, accessed on 23 March 2023). The satellite SST, SSH, and in situ temperature and salinity, as well as the sea ice concentration and thickness, were assimilated into the product via the Nucleus for European Modelling of the Ocean 1/12° global model (NEMO version 3.1), with 50 vertical levels and 1/12° horizontal resolution. As indicated in Figure 1, the CMEMS SSS closely matches the SMOS SSS, exhibiting a correlation coefficient as high as 0.95 during 2010–2020. Therefore, the CMEMS salinity and currents were utilized for the analysis in this study. The CMEMS salinity and current anomaly were measured on the basis of the 28-year mean daily climatology (1993–2020).

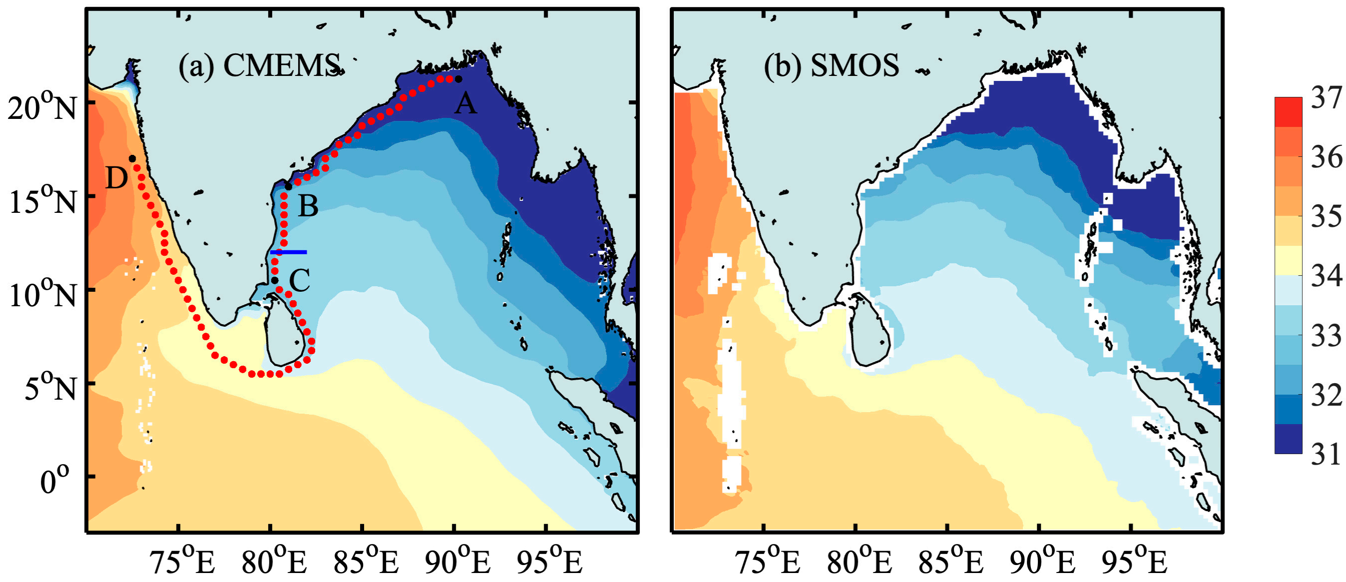

Figure 1. Climatological (**a**) CMEMS and (**b**) SMOS SSS (psu) data in the BoB for the period of 2010–2020. The red dots represent the trajectory originating from the northern BoB, moving along the eastern coast of India, and ultimately reaching the western coast of India. The dot A, B, C, and D located in the northern BoB, western BoB, northern tip of Sri Lanka and western coast of India, respectively. The blue line indicates the section at 12°N, 80–82°E.

The gridded daily sea level anomalies (SLAs) and the geostrophic zonal and meridional currents with spatial resolutions of 1/4° × 1/4°, obtained from the Archiving, Validation, and Interpretation of Satellite Oceanographic data (AVISO, https://www.aviso.altimetry.fr/ accessed on 20 March 2023) and distributed by the CMEMS (DOI: https://doi.org/10.48670/moi-00148 accessed on 20 March 2023), were used to characterize the processes of oceanic Kelvin and Rossby waves. The SLA data have been available since 1993 and is computed with respect to the 1993–2012 mean sea surface height (SSH). The product contains merged data from all altimetry satellite missions (the European Remote Sensing Satellite (ERS-1/2), Jason-1&2, Jason-3, Ocean Topography Experiment (TOPEX)/Poseidon, Envisat, Sentinel-3A, Saral, Geosat, Geosat Follow-On (GFO), and Cryosat-2). To remove the influence of global warming on SLAs, we removed the 28-year daily trend (1993–2020) from the SLA data.

A detailed summary of the datasets used in the present study is given in Table 1.

Table 1. Summary of the datasets used in this study.

Parameter	Source	Resolution	Time Period
Zonal wind at 10 m	https://cds.climate.copernicus.eu accessed on 10 April 2023	Hourly, 0.25° × 0.25°	1991–2021
SMOS SSS	https://earth.esa.int/ accessed on 15 April 2022	Every 4 days, 25 × 25 km^2	2010–2020
CMEMS current, salinity, and potential temperature	http://marine.copernicus.eu accessed on 23 March 2023	Daily, 1/12° × 1/12°, 50 vertical levels	1993–2020
AVISO SLA, geostrophic zonal and meridional currents	https://www.aviso.altimetry.fr/ accessed on 20 March 2023	Daily, 0.25° × 0.25°	1993–2020

2.2. Methods

To measure the strength of the westerlies over the EIO, we defined a westerly index (WI) based on the area-averaged zonal wind anomaly in the EIO (1°S–1°N, 70–90°E). The zonal wind anomaly was calculated relative to a monthly climatological seasonal cycle based on the years 1991–2021. WI > 0 indicates an intensification of westerlies in comparison to the seasonal climatology. WI < 0 suggests a relatively weaker westerly pattern compared to the seasonal climatology or, alternatively, indicates easterly winds prevailing over the EIO.

The standardized value of the WI is computed using the following equation [21]:

$$Z = \frac{X - \mu}{\sigma} \tag{1}$$

where μ is the mean value of the WI time series, σ is the standard deviation of the WI time series, X is the WI time series, and Z is the standardized value of the WI.

We employed canonical linear correlation and regression analysis to find statistical relationships between CMEMS SSS anomalies and the WI. Student's t test was applied to assess the statistical significance of the correlation and regression analysis.

3. Results

3.1. Regression and Correlation Analysis

Regression and correlation analysis is necessary for understanding the link between the equatorial zonal wind and the distribution of SSSAs in the BoB. During the fall transition between the summer and winter monsoons, the zonal winds are mostly westerlies in the equatorial Indian Ocean [11]. To measure the strength of the westerlies, we defined the westerly index (WI). A regression analysis between CMEMS SSSAs from October to December (OND) within the BoB and the WI from August to November (ASON) revealed the imprint of interannual variation in the zonal wind in the EIO on the distribution of salinity in the BoB (Figure 2). A positive regression coefficient value indicates that a positive WI (strong westerlies) induces positive SSSAs and a negative WI (weak westerlies or easterlies) induces negative SSSAs. A negative regression coefficient value indicates that a positive WI induces negative SSSAs and negative WI induces a positive SSSAs. The regression coefficient was relatively significant in the eastern EIO and along the coast of the BoB (Figure 2).

Four areas in which the SSSA variation is prominently influenced by the WI were chosen to analyze the lead–lag correlation between the monthly WI and OND SSSAs in the BoB. Area 1 in the eastern EIO (0°N–5°N, 85–95°E), area 2 in the Andaman Sea (8–14°N, 94.5–97.5°E), area 3 in the northern BoB (18–22°N, 88–93°E), and area 4 in the western BoB (5–15°N, 79–83°E) are shown in Figure 2. As shown in Figure 3, the correlations between OND SSSAs in these four areas and the monthly WI were notably high from August to November, except for in area 3 (Figure 3c). An above-normal WI from August to November would trigger a positive OND SSSA in the eastern EIO and Andaman Sea while simultaneously causing a negative SSSA in the western BoB. However, there was no significant correlation between the OND SSSAs in the northern BoB and the WI throughout the year, which may be related to the fact that the interannual variation in the salinity anomaly in the northern BoB is more significant, affected by monsoon precipitation and runoff [22].

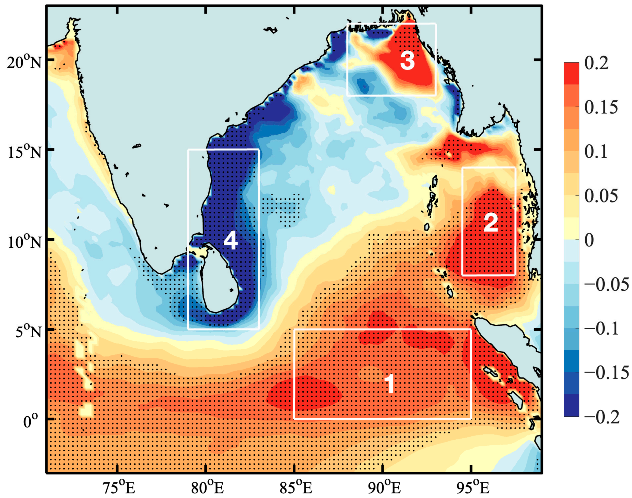

Figure 2. The regression patterns of OND CMEMS SSSAs against the ASON westerly index (WI) over the 1993–2020 period. White boxes represent area 1 in the eastern EIO (0°N–5°N, 85–95°E), area 2 in the Andaman Sea (8–14°N, 94.5–97.5°E), area 3 in the northern BoB (18–22°N, 88–93°E) and area 4 in the western BoB (5–15°N, 79–83°E). Black dots represent grid points with statistical significance exceeding the 99% confidence level.

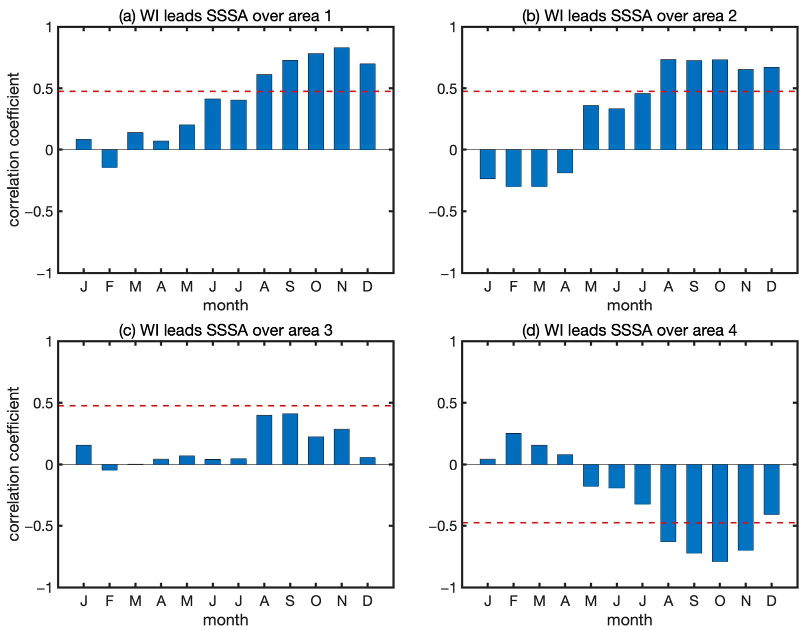

Figure 3. Lead–lag correlation between the monthly westerly index (WI) and area–averaged OND SSSAs in the Bay of Bengal for the period of 1993–2020 in (**a**) area 1: 0°N–5°N, 85–95°E; (**b**) area 2: 8–14°N, 94.5–97.5°E; (**c**) area 3: 15–22°N, 85–93°E; (**d**) area 4: 5–15°N, 79–83°E.

We referred to the years with a standardized value of the August–November WI time series above +1 as "anomalous westerly" years (2010 and 2016) and those with a value below −1 as "anomalous easterly" years (1994, 1997, 2006, and 2019) from the reference period of 1991–2021 (Figure 4). It is worth noting that the co-occurrence of negative-IOD and La Niña events took place in 2010 and 2016, while positive-IOD events coincided with

El Niño occurrences in 1994, 1997, and 2006. Furthermore, an exceptionally strong positive IOD event was observed in 2019 [23,24]. In fact, during anomalous easterly years, the zonal wind exhibited easterlies, with particularly strong easterlies observed in 1997 and 2019 (exceeding a velocity of 2 m/s). In the following paragraph, we further analyze the characteristics of the distribution of SSSAs in the BoB in each anomalous westerly year and each anomalous easterly year.

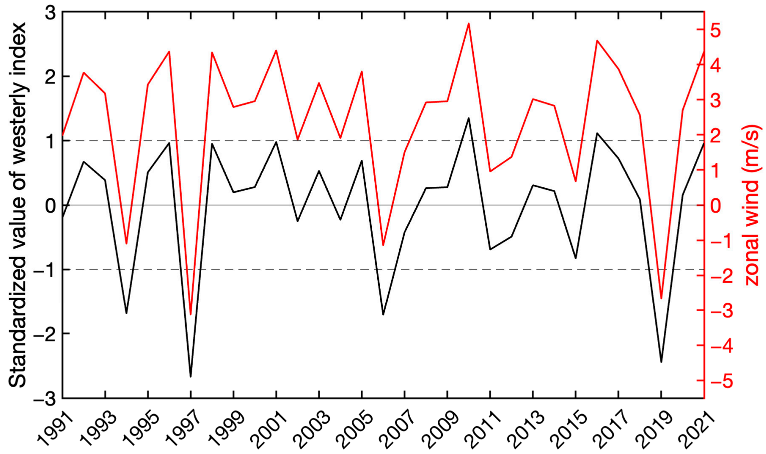

Figure 4. Standardized values of the westerly index (black line) and zonal wind speed (m/s) over the equatorial Indian Ocean (red line; 1°S–1°N, 70–90°E).

3.2. Characteristics of SSSAs in Anomalous Westerly Years and Easterly Years

As shown in Figure 5a, the salinity in the BoB exhibited a significant contrast to that observed in the Arabian Sea and western EIO, characterized by a notably lower SSS. The SSS in the northern Andaman Sea, in the northern BoB, and along the coastal region of eastern India was as low as 31 psu from October to December in the climatology.

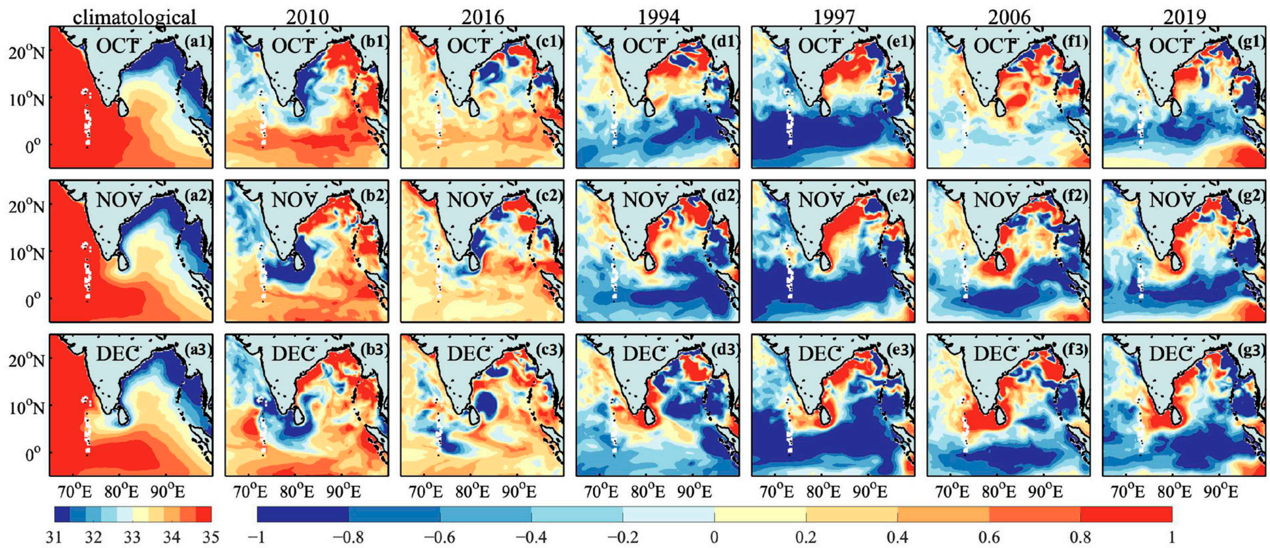

Figure 5. Distribution of the climatological monthly CMEMS SSS (**a1**–**a3**) and interannual anomalous SSS in 2010 (**b1**–**b3**), 2016 (**c1**–**c3**), 1994 (**d1**–**d3**), 1997 (**e1**–**e3**), 2006 (**f1**–**f3**), and 2019 (**g1**–**g3**) in October (the first row), November (the second row), and December (the third row).

The distribution of salinity anomalies in the years characterized by westerly and easterly anomalies from October to December exhibits a remarkably different pattern (Figure 5). Particularly in the eastern EIO and most parts of the Andaman Sea, the SSSA was positive in 2010 and 2016, while negative SSSAs were observed in 1994, 1997, 2006, and

2019. Furthermore, the notably negative (positive) SSSAs observed in the northwestern BoB in October 2010 and 2016 (1994, 1997, 2006, and 2019) gradually extended southward along the eastern coast of India over time before reaching Sri Lanka by December. However, the distinction of SSSAs in the northern BoB was not evident in anomalous westerly years and anomalous easterly years. In October 2010, a positive SSSA in the Andaman Sea was consecutive to a patch of positive SSSA in the northern BoB. Subsequently, the positive SSSA in the northern BoB extended southward. In contrast to October 2010, a positive SSSA in the southern Andaman Sea and northern BoB was disrupted by a negative SSSA in the northern Andaman Sea in October 2016. The SSSA pattern in the northeastern BoB was not unified in 1994, 1997, 2006, and 2019.

To further investigate the southward movement of SSSAs in the northwestern BoB, we established a transect spanning across the northern BoB, along the eastern coast of India, and ultimately reaching the western coast of India (red dots in Figure 1a). As shown in Figure 6, the negative (positive) SSSA signal in the northwestern BoB (between point A and B) in October 2010 (1994, 1997, 2006, and 2019) propagated southward along the eastern coast of India, passed Sri Lanka, and arrived on the western Indian coast in December. The negative SSSA signal in October 2016 could only propagate as far as Sri Lanka.

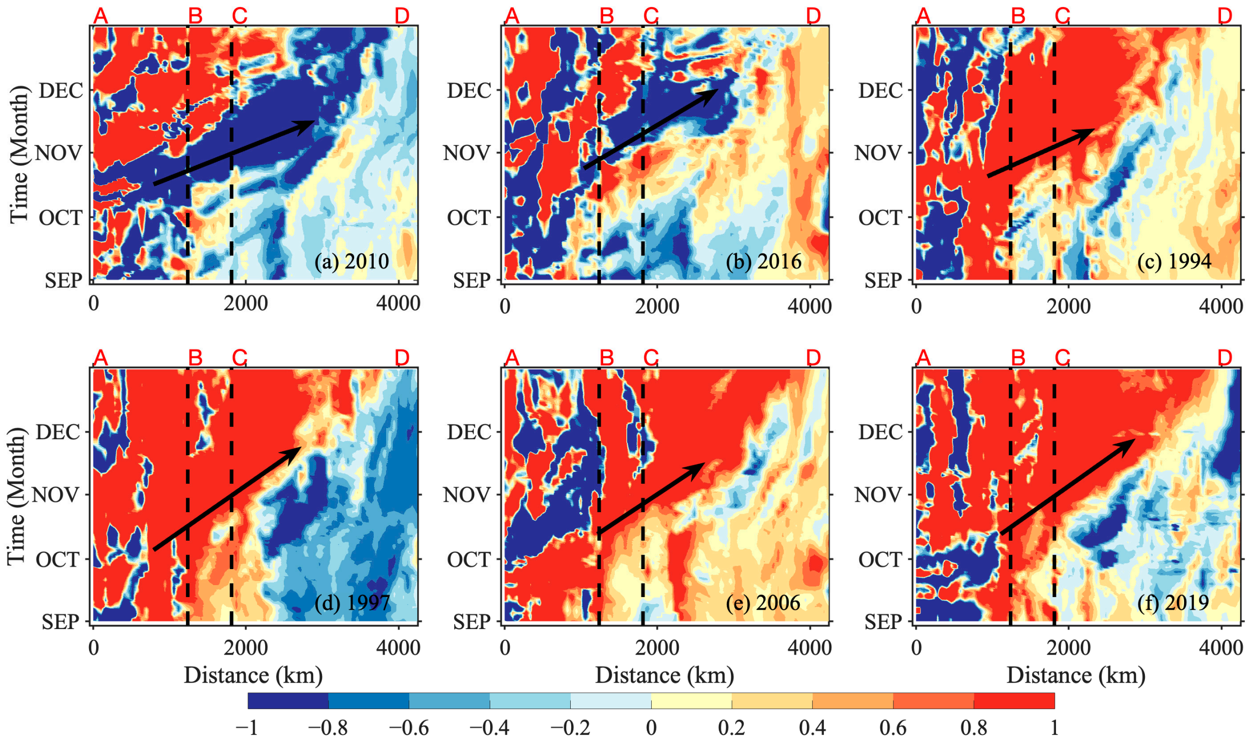

Figure 6. Time–distance plot of the CMEMS SSSAs (psu) from September to December along the red dots in Figure 1a in (**a**) 2010, (**b**) 2016, (**c**) 1994, (**d**) 1997, (**e**) 2006, and (**f**) 2019. The dot A, B, C, and D located in the northern BoB, western BoB, northern tip of Sri Lanka and western coast of India, respectively. The dot lines mark the distance of dot B and C. The arrows indicate the movement of salinity anomalies.

As mentioned above, the distribution of salinity anomalies in the years characterized by westerly and easterly anomalies from October to December demonstrates notable disparities. At this point, the following question arises: what is the connection between equatorial zonal winds and salinity anomalies in the BoB? To answer this question, the link between SSSAs in the BoB and anomalous zonal winds in the EIO, along with the corresponding mechanisms, is discussed in the next paragraph.

3.3. Large-Scale Currents

As shown in Figure 3, equatorial zonal winds from August are highly correlated with OND salinity anomalies in the eastern EIO, Andaman Sea, and western BoB. Previous studies have demonstrated that the interannual variability of salinity in the BoB in the boreal fall mainly arises from horizontal currents associated with the IOD and ENSO [1,6,8,25]. Therefore, it is necessary to analyze the anomalous currents at the equator and in the BoB from August to December.

As depicted in Figure 7, during August–September in both 2010 and 2016, the presence of anomalous westerlies along the equator resulted in the occurrence of anomalous eastward currents. Following the anomalous eastward currents, more high-salinity water from the western EIO moved to the eastern EIO and BoB, thereby contributing to the existence of a positive SSSA in the eastern EIO and Andaman Sea. A reverse pattern was observed in 1994 and 1997.

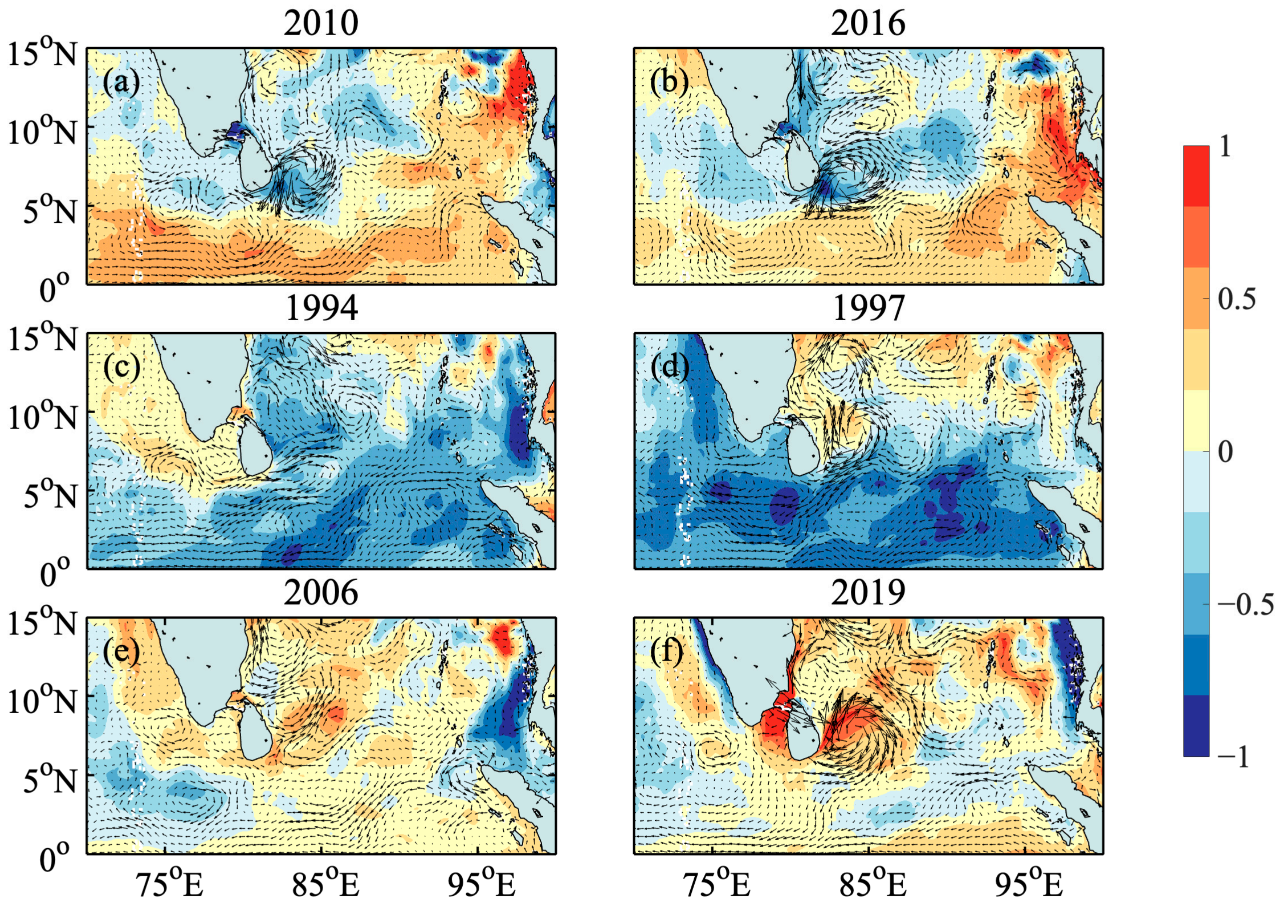

Figure 7. August–September averaged CMEMS SSSAs (psu; shaded) and anomalous surface currents (m/s; vector) in (**a**) 2010, (**b**) 2016, (**c**) 1994, (**d**) 1997, (**e**) 2006, and (**f**) 2019.

As shown in Figure 8a, consistent with previous research, climatological westerlies prevailing over the EIO drive the eastward Wyrtki jet along the equator during OND. Upon reaching the Sumatra coast, a portion of these currents flows into the BoB [11,12]. Thus, high-salinity waters from the western EIO move eastward, and parts of them bifurcate northward into the BoB. A basin-scale cyclonic circulation is observed in the BoB. At the western boundary of the BoB, freshwater from the northern BoB flows southward via the EICC along the eastern coast of India.

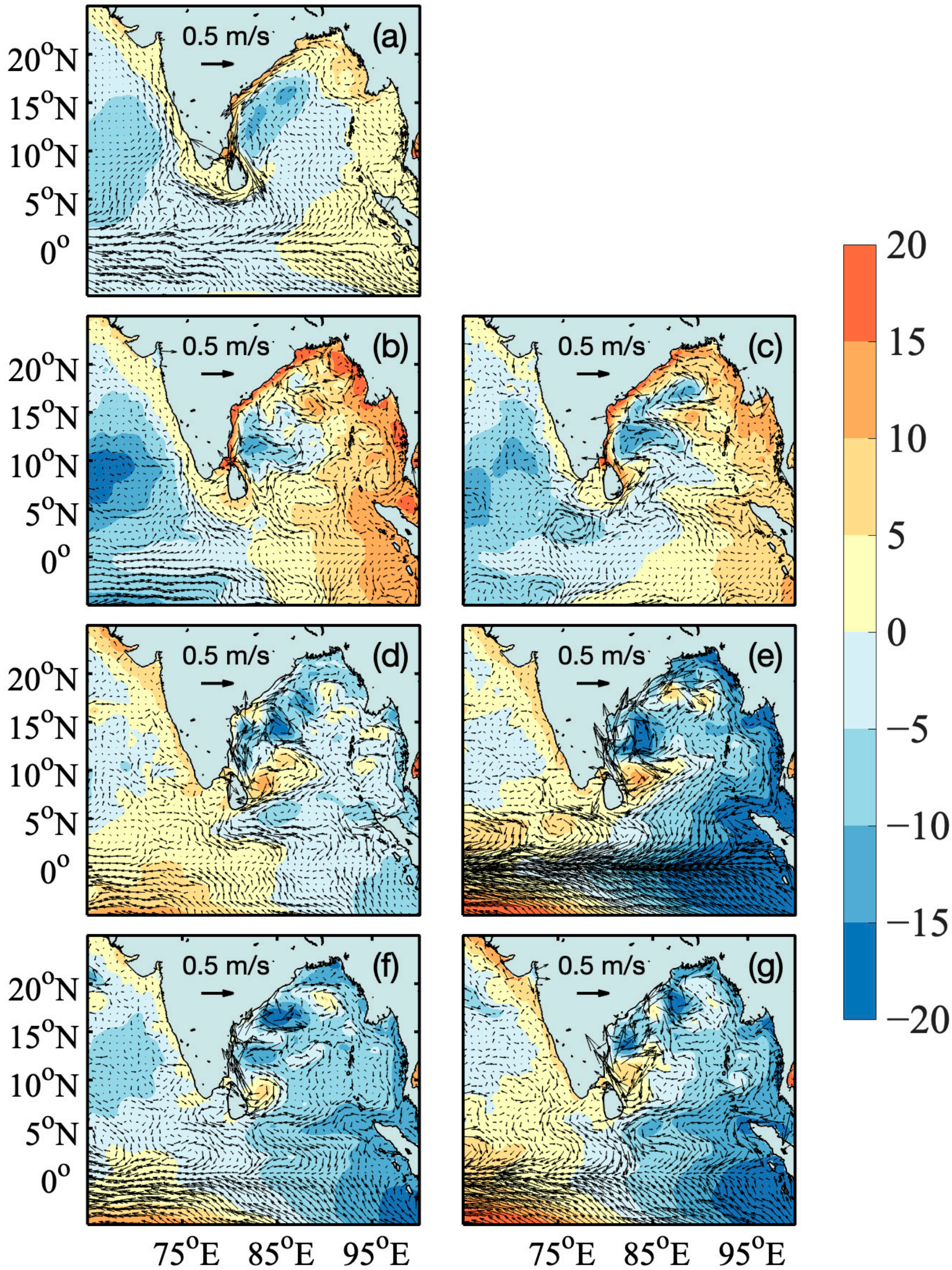

Figure 8. (**a**) October–December averaged AVISO sea level anomalies (SLAs; shaded) and geostrophic currents (m/s; vector) in the local climatology. October–December averaged AVISO SLAs and anomalous geostrophic currents in (**b**) 2010, (**c**) 2016, (**d**) 1994, (**e**) 1997, (**f**) 2006, and (**g**) 2019.

As shown in Figure 8b–g, distinctive dissimilarities in anomalous surface currents during OND were observed in anomalous westerly years (2010 and 2016) and anomalous easterly years (1994, 1997, 2006, and 2019). The Wyrtki jet was anomalously westward in 1994, 1997, 2006, and 2019, which was conducive to the negative SSSA in the eastern EIO. During OND 2010 and 2016 (1994, 1997, 2006, and 2019), the anomalous northward (southward) currents in the southern BoB flowed northward into (southward out of) the Andaman Sea and contributed to the increased (decreased) northward movement of high-salinity water, resulting in a positive (negative) SSSA in both regions. In addition, there was an anomalous basin-scale cyclonic (anticyclonic) circulation in the BoB, resulting in increased high-salinity (low-salinity) water flowing northward (southward) and a positive (negative) SSSA along the eastern BoB. Thus, both the reduced northward movement of high-salinity water associated with the Wyrtki jet and the increased southward freshwater associated with anomalous anticyclonic circulation contributed to the negative salinity anomaly in the Andaman Sea and eastern EIO. Simultaneously, the EICC was stronger (weaker) compared to the local climatology. Thus, increased (decreased) freshwater flow southward along the eastern coast of India and the southward movement of a negative (positive) SSSA were observed in OND 2010 and 2016 (1994, 1997, 2006, and 2019).

To further explore the strength of the Wyrtki jet and EICC, a depth–longitude plot of zonal currents along the equator and meridional currents along the 12°N section is shown in Figures 9 and 10, respectively. In the climatology, as shown in Figure 9a, driven by prevailing westerlies over the EIO, the October–November Wyrtki jet is mainly confined to the upper 80 m, with speeds often exceeding 0.5 m/s. In anomalous westerly years, the Wyrtki jet in the upper 70 m experienced an amplification of 0.2 m/s, with velocities surpassing 0.7 m/s (Figure 9b,c,h,i). In the years 1994, 1997, 2006, and 2019, the easterly winds exceeded a velocity of 1 m/s (Figure 4), resulting in the absence of eastward Wyrtki jets. During October–November 1994, 1997, 2006, and 2019, the zonal currents along the equator were westward (Figure 9e–g), with the anomalous currents reaching a speed of 0.5 m/s in the upper 50 m (Figure 9j–m). Thus, the strengthened (weakened or absent) eastward Wyrtki jet contributed to the positive (negative) SSSA in the eastern EIO and Andaman Sea in anomalous westerly (easterly) years. The climatological speed of the EICC in the upper 50 m exceeded 0.5 m/s (Figure 10a). The EICC was strengthened in anomalous westerly years, especially in 2010. The EICC in 2010 experienced an amplification of 0.2 m/s within the uppermost 50 m, with velocities exceeding 0.7 m/s (Figure 10b,h). In contrast, the EICC was weakened in 1994, 1997, and 2006 (Figure 10d–f,j–l). Particularly, the EICC was northward in 2019 at a velocity surpassing 0.1 m/s (Figure 10g). Therefore, the strengthened (weakened or absent) southward EICC contributed to the southward movement of negative (positive) SSSAs along the eastern coast of India in anomalous westerly (easterly) years.

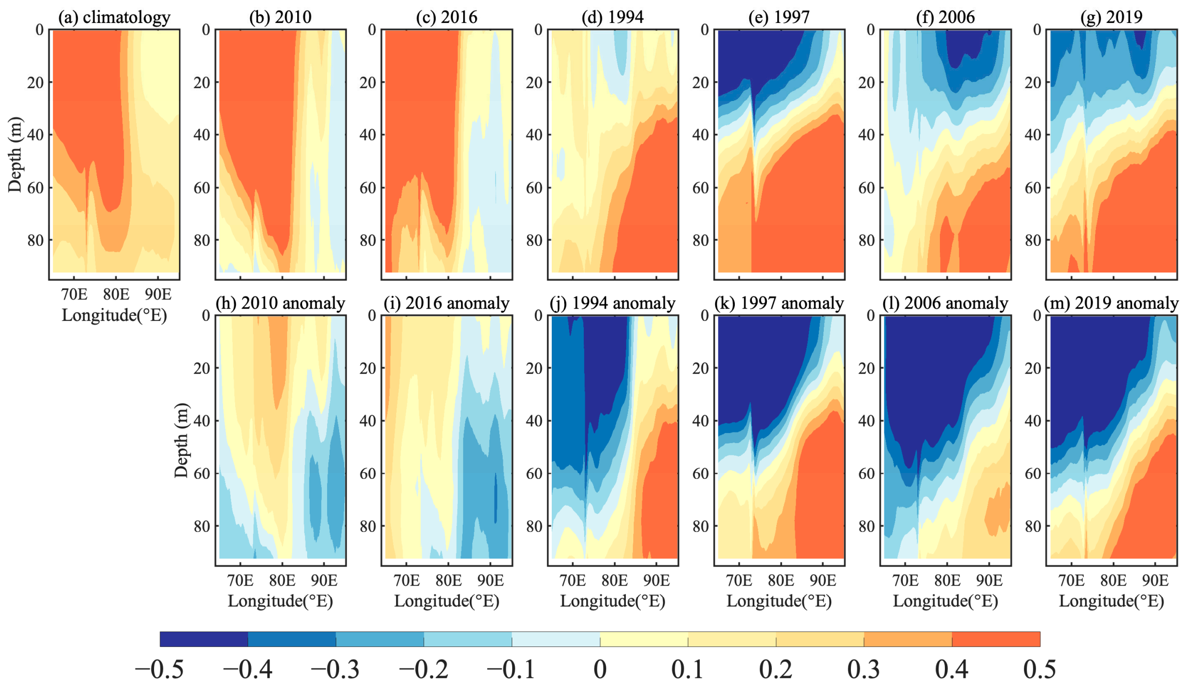

Figure 9. Depth–longitude plot of the October–November averaged zonal currents along the equator (m/s) in (**a**) the local climatology, (**b**) 2010, (**c**) 2016, (**d**) 1994, (**e**) 1997, (**f**) 2006, and (**g**) 2019 and anomalies in (**h**) 2010, (**i**) 2016, (**j**) 1994, (**k**) 1997, (**l**) 2006, and (**m**) 2019.

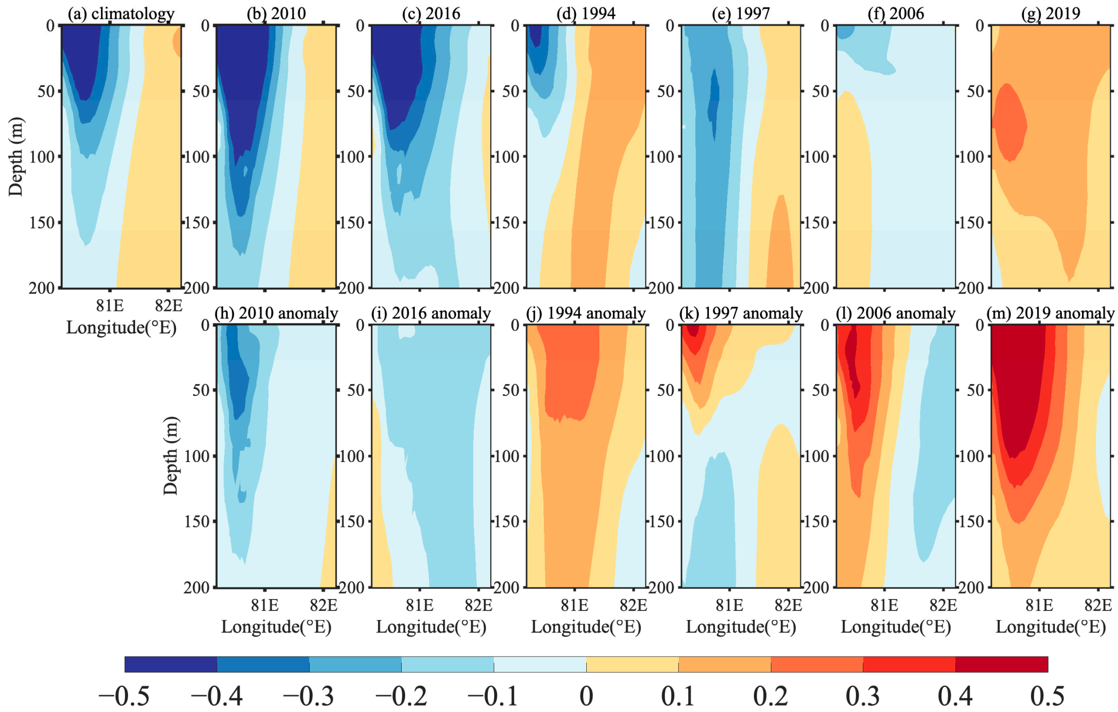

Figure 10. Depth–longitude plot of October–December averaged meridional currents (m/s) along the 12°N section (blue line in Figure 1a) in (**a**) the local climatology, (**b**) 2010, (**c**) 2016, (**d**) 1994, (**e**) 1997, (**f**) 2006, and (**g**) 2019 and anomalies in (**h**) 2010, (**i**) 2016, (**j**) 1994, (**k**) 1997, (**l**) 2006, and (**m**) 2019.

3.4. Kelvin Waves

The strengthened (weakened) Wyrtki jet in 2010 and 2016 (1994, 1997, 2006, and 2019) was attributed to the anomalous westerlies (easterlies) over the EIO. However, how did the westerlies over the EIO influence the currents in the BoB?

Previous studies have demonstrated that, from October to December, climatological westerlies over the EIO activate the eastward equatorial downwelling Kelvin waves [16]. Upon hitting the Sumatra coast, these waves bifurcate northward and transform into coastal downwelling Kelvin waves along the coast of the BoB in October, then pass Sri Lanka and arrive at the western coast of India in November. These downwelling Kelvin waves deepen the thermocline and are associated with positive SLAs. The positive SLAs along the rim of the BoB contribute to the basin-scale cyclonic circulation in the BoB (Figure 8a). Consequently, high-salinity waters from the EIO move into the eastern BoB, and a large amount of freshwater from the northern BoB flows southward via the EICC.

As shown in Figures 8 and 10, strengthened coastal downwelling Kelvin waves were observed in OND 2010 and 2016, leading to anomalous cyclonic basin-scale circulation along the rim of the BoB and an intensified southward EICC, giving rise to the southward movement of negative SSSAs along the eastern coast of India. In contrast, coastal upwelling contributed to anomalous anticyclonic circulation along the rim of the BoB and a weak southward (northward) EICC in 1994, 1997, and 2006 (2019), resulting in the southward movement of positive SSSAs along the eastern coast of India. It is worth noting that the upwelling Kelvin waves in anomalous easterly years could propagate only as far as the east coast of India (Figure 8d–g). The disruption in the propagation of negative SLA signals was attributed to the anticyclonic mesoscale eddy located on the eastern coast of Sri Lanka. In conclusion, zonal winds over the EIO and Kelvin waves exert a significant influence on large-scale circulation, subsequently influencing the distribution of salinity within the BoB.

3.5. Rossby Waves

The northward propagation of coastal Kelvin waves excites the westward propagation of Rossby waves, which subsequently propagate into the interior of the BoB [26]. In this context, it is imperative to explore the potential contribution of the Rossby waves to the spatial distribution of salinity within the BoB. Figure 11 depicts the temporal evolution of the SLAs at section 10°N, SSSAs at section 10°N, SLAs at section 15°N, and SSS at section 15°N. The black dotted arrow in each panel indicates the westward propagation signal. It is clear that the SLAs showed positive (negative) values with a westward-propagating signature in 2010 and 2016 (1994, 1997, 2006, and 2019) at sections 10°N and 15°N. The mean propagation speeds of the Rossby waves, calculated based on the wave pattern slopes at 10°N and 15°N, were estimated to be approximately 19.19 cm/s and 8.98 cm/s, respectively, which are comparable to the theoretical phase speeds (approximately 22cm/s at 10°N and 10 cm/s at 15°N) of Rossby waves at these latitudes [27]. As evident from Figure 11, when the westward propagation of Rossby waves occurred, both the signals of the SSSAs at section 10°N and the SSS at section 15°N in the BoB exhibited the corresponding characteristics of westward propagation. The westward positive (negative) SSSA at section 10°N could counteract the negative (positive) SSSA along the eastern Indian coast in anomalous westerly (easterly) years. On the other hand, due to substantial river runoff from the Irrawaddy River, the salinity in the east of section 15°N is notably low. Thus, the westward movement of low-salinity water at section 15°N plays a crucial role in maintaining the salinity balance in the northeastern BoB. In summary, the westward salinity signal associated with Rossby waves could modulate the redistribution of salinity.

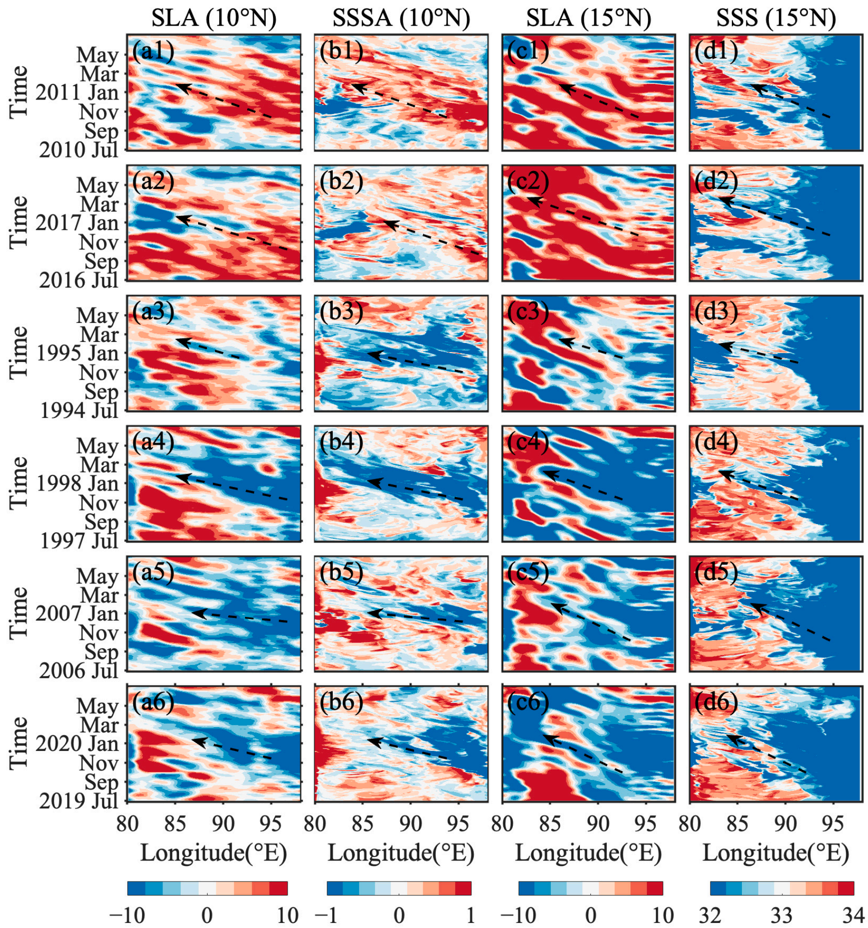

Figure 11. Time–longitude plot of (**a1**–**a6**) AVISO SLAs (cm) and (**b1**–**b6**) CMEMS SSSAs (psu) along the 10°N section. Time–longitude plot of (**c1**–**c6**) AVISO SLAs and (**d1**–**d6**) CMEMS SSS (psu) along the 15°N section. The arrows indicate the westward propagation signal.

4. Discussion

Our study explored the connection between zonal winds in the EIO and activated Kelvin waves, modulated by the IOD and ENSO, and the interannual variations in the salinity distribution in the BoB during OND, along with its associated dynamics, using satellite and reanalysis datasets. According to the strength of zonal winds over the EIO during August–November, we selected two extreme westerly years (2010 and 2016) alongside four notable anomalous easterly years (1994, 1997, 2006, and 2019). Our analysis shows that the distributions of salinity anomalies during years characterized by westerly and easterly anomalies exhibit distinctly different patterns. In OND 2010 and 2016 (1994, 1997, 2006, and 2019), positive (negative) SSSAs were distributed in the eastern EIO and Andaman Sea; moreover, the southward movement of negative (positive) SSSAs along the eastern Indian coast was observed. Large-scale anomalous currents associated with zonal winds over the EIO contributed to this phenomenon. During OND 2010 and 2016 (1994, 1997, 2006, and 2019), due to anomalous westerlies (easterlies) over the EIO and anomalous downwelling (upwelling) Kelvin waves, the strengthened (weakened) Wyrtki jet and the basin-scale anomalous cyclonic (anticyclonic) circulation in the BoB led to positive (negative) SSSAs within the eastern EIO and Andaman Sea. In addition, the enhanced (diminished) EICC contributed to the southward movement of negative (positive) SSSAs.

It is worth noting that downwelling Kelvin waves could reach the western coast of India during anomalous westerly events, while upwelling Kelvin waves are confined to the eastern coast of India during anomalous easterly events. On the other hand, the northward propagation of coastal Kelvin waves excites westward-propagating Rossby waves, which subsequently propagate into the interior of the BoB. When the westward propagation of Rossby waves occurred, the signals of SSSAs at section 10°N and of SSS at section 15°N in the BoB both exhibited the corresponding characteristics of westward propagation. The westward positive (negative) SSSA at section 10°N could counteract the negative (positive) SSSA along the eastern Indian coast in anomalous westerly (easterly) years. The westward low-salinity water at section 15°N plays a crucial role in maintaining the salinity balance in the northwestern BoB. The westward signals of SSS at section 15°N and SSSAs at section 10°N associated with reflected westward Rossby waves could modulate the redistribution of salinity.

However, the physical mechanisms underlying the impact of Rossby waves on the westward propagation of salinity signals remain elusive. Two channels connect the Andaman Sea and the BoB at 10°N and 15°N [14]. The channel at 10°N separates the Andaman Islands and Nicobar Islands, while the northern boundary of the channel at 15°N is located at the tip of the Irrawaddy Delta off Myanmar. The Rossby waves could pass through the Andaman Sea to the BoB via these channels and influence the circulation in the BoB [28]. According to previous studies, the Rossby waves, reflected by coastal Kelvin waves at the eastern boundary of the BoB, manifest as eddy-like SLAs and propagate westward [29–31]. Thus, in our study, the westward propagation signals of low salinity at 15°N and the salinity anomaly at 10°N were likely attributed to the westward movement of eddy-like currents associated with Rossby waves. The eddy-like currents trapped the low-salinity water and salinity anomalies within their circulation and moved westward, which could have modulated the redistribution of salinity within the BoB.

In our study, positive (negative) SSSAs in the eastern EIO and Andaman Sea and the southward movement of negative (positive) SSSAs along the eastern coast of India were observed during OND in anomalous westerly (easterly) years. These salinity anomalies could influence air–sea interactions. Strong salinity stratification manifests as a shallow mixed-layer depth and a thick barrier layer. The thick barrier layer acts to suppress turbulent vertical transfers between the mixed layer and the thermocline [32,33]. In the presence of a shallow mixed layer and thick barrier layer, incoming heat fluxes can be trapped within the shallow mixed layer, consequently influencing sea surface temperature variability [34]. Ivanova et al. [35] demonstrated that the thick barrier layer in the eastern EIO, west of Sumatra, during November–January intensifies local convection and amplifies the moisture transport to Australia, thereby acting to increase the terrestrial rainfall. Thus, positive (negative) SSSAs in the eastern EIO in the anomalous westerly (easterly) years could potentially suppress the formation of a thick barrier layer and rainfall in Australia. In addition, salinity anomalies along the eastern coast of India subsequently propagated around Sri Lanka and extended further into the southeast Arabian Sea through the western Indian coastal current. Salinity variations in the southeast Arabian Sea could influence the salinity stratification there, thereby impacting the formation of the barrier layer in winter and subsequent variations in the Arabian Sea mini warm pool in the following spring [36].

Author Contributions: Conceptualization, F.Q.; methodology, F.Q. and S.C.; validation, F.Q.; formal analysis, S.C. and F.Q.; data curation, F.Q. and S.C.; writing—original draft preparation, S.C.; writing—review and editing, S.C., F.Q., C.J., Y.Q. and J.Z.; visualization, S.C.; funding acquisition, F.Q. and Y.Q. All authors have read and agreed to the published version of the manuscript.

Funding: This work was funded by the Scientific Research Foundation of the Third Institute of Oceanography, MNR (Grant numbers: 2022021), the National Natural Science Foundation of China (42130406), the Global Change and Air-Sea Interaction II Program (GASI-04-WLHY-03, GASI-04-QYQH-01; GASI-01-SIND-STwin), and the National Key Research and Development Program of China (2016YFC1402607).

Data Availability Statement: The SMOS sea surface salinity data were obtained at https://earth.esa.int/, accessed on 15 April 2022. The ERA5 dataset was obtained at https://cds.climate.copernicus.eu/, accessed on 10 April 2023. The CMEMS dataset was obtained at http://marine.copernicus.eu, accessed on 23 March 2023. The AVISO dataset was obtained at https://www.aviso.altimetry.fr/, accessed on 20 March 2023.

Acknowledgments: We would like to thank the reviewers for their time spent on reviewing our manuscript and their comments helping us to improve the article.

Conflicts of Interest: The authors declare no conflicts of interest.

References

1. Li, Z.; Lian, T.; Ying, J.; Zhu, X.; Papa, F.; Xie, H.; Long, Y. The Cause of an Extremely Low Salinity Anomaly in the Bay of Bengal During 2012 Spring. *J. Geophys. Res. Ocean.* **2021**, *126*, e2021JC017361. [CrossRef]
2. Sprintall, J.; Tomczak, M. Evidence of the barrier layer in the surface layer of the tropics. *J. Geophys. Res.* **1992**, *97*, 7305–7316. [CrossRef]
3. Thadathil, P.; Muraleedharan, P.M.; Rao, R.R.; Somayajulu, Y.K.; Reddy, G.V.; Revichandran, C. Observed seasonal variability of barrier layer in the Bay of Bengal. *J. Geophys. Res.* **2007**, *112*. [CrossRef]
4. Cronin, M.F.; McPhaden, M.J. Barrier layer formation during westerly wind bursts. *J. Geophys. Res. Ocean.* **2002**, *107*, SRF 21-1–SRF 21-12. [CrossRef]
5. Rao, R.R. Seasonal variability of sea surface salinity and salt budget of the mixed layer of the north Indian Ocean. *J. Geophys. Res.* **2003**, *108*, 9-1–9-14. [CrossRef]
6. Akhil, V.P.; Valiya Parambil, A.; Valiya Parambil, A.; Matthieu, L.; Jérôme, V.; Fabien, D.; Fabien, D.; Keerthi, M.G.; Akurathi Venkata Sai, C.; Fabrice, P.; et al. A modeling study of processes controlling the Bay of Bengal sea surface salinity interannual variability. *J. Geophys. Res.* **2016**, *116*, 3926–3947. [CrossRef]
7. Akhil, V.P.; Vialard, J.; Lengaigne, M.; Keerthi, M.G.; Boutin, J.; Vergely, J.L.; Papa, F. Bay of Bengal Sea surface salinity variability using a decade of improved SMOS re-processing. *Remote Sens. Environ.* **2020**, *248*, 111964. [CrossRef]
8. Chen, S.; Cha, J.; Qiu, F.; Jing, C.; Qiu, Y.; Xu, J. Sea Surface Salinity Anomaly in the Bay of Bengal during the 2010 Extremely Negative IOD Event. *Remote Sens.* **2022**, *14*, 6242. [CrossRef]
9. Chaitanya, A.V.S.; Durand, F.; Mathew, S.; Gopalakrishna, V.V.; Papa, F.; Lengaigne, M.; Vialard, J.; Kranthikumar, C.; Venkatesan, R. Observed year-to-year sea surface salinity variability in the Bay of Bengal during the 2009–2014 period. *Ocean Dyn.* **2014**, *65*, 173–186. [CrossRef]
10. Zhang, Z.; Wang, J.; Yuan, D. Mixed Layer Salinity Balance in the Eastern Tropical Indian Ocean. *J. Geophys. Res. Ocean.* **2022**, *127*, e2021JC018229. [CrossRef]
11. Wyrtki, K. An equatorial jet in the Indian Ocean. *Science* **1973**, *181*, 262–264. [CrossRef]
12. Jing, W.; Jing, W.; Jing, W. Observational bifurcation of Wyrtki Jets and its influence on the salinity balance in the eastern Indian Ocean. *Atmos. Ocean. Sci. Lett.* **2017**, *10*, 36–43. [CrossRef]
13. Thompson, B.; Gnanaseelan, C.; Salvekar, P.S. Variability in the Indian Ocean circulation and salinity and its impact on SST anomalies during dipole events. *J. Mar. Res.* **2006**, *64*, 853–880. [CrossRef]

14. Chatterjee, A.; Shankar, D.; McCreary, J.P.; Vinayachandran, P.N.; Mukherjee, A. Dynamics of Andaman Sea circulation and its role in connecting the equatorial Indian Ocean to the Bay of Bengal. *J. Geophys. Res. Ocean.* **2017**, *122*, 3200–3218. [CrossRef]
15. Yu, L.; O'Brien, J.J.; Yang, J. On the remote forcing of the circulation in the Bay of Bengal. *J. Geophys. Res.* **1991**, *96*, 20449–20454. [CrossRef]
16. Rao, R.R.; Girish Kumar, M.S.; Ravichandran, M.; Rao, A.R.; Gopalakrishna, V.V.; Thadathil, P. Interannual variability of Kelvin wave propagation in the wave guides of the equatorial Indian Ocean, the coastal Bay of Bengal and the southeastern Arabian Sea during 1993–2006. *Deep Sea Res. Part I Oceanogr. Res. Pap.* **2010**, *57*, 1–13. [CrossRef]
17. Fournier, S.; Vialard, J.; Lengaigne, M.; Lee, T.; Gierach, M.M.; Chaitanya, A.V.S. Modulation of the Ganges-Brahmaputra River Plume by the Indian Ocean Dipole and Eddies Inferred From Satellite Observations. *J. Geophys. Res. Ocean.* **2017**, *122*, 9591–9604. [CrossRef]
18. Sreenivas, P.; Gnanaseelan, C.; Prasad, K.V.S.R. Influence of El Niño and Indian Ocean Dipole on sea level variability in the Bay of Bengal. *Glob. Planet. Chang.* **2012**, *80–81*, 215–225. [CrossRef]
19. Pant, V.; Girishkumar, M.S.; Bhaskar, T.V.S.U.; Ravichandran, M.; Fabrice, P.; Thangaprakash, V.P. Observed interannual variability of near-surface salinity in the Bay of Bengal. *J. Geophys. Res.* **2015**, *120*, 3315–3329. [CrossRef]
20. Hersbach, H.; Bell, B.; Berrisford, P.; Biavati, G.; Horányi, A.; Muñoz Sabater, J.; Nicolas, J.; Peubey, C.; Radu, R.; Rozum, I.; et al. ERA5 Hourly Data on Single Levels from 1940 to Present; Copernicus Climate Change Service (C3S) Climate Data Store (CDS). 2023. Available online: https://cds.climate.copernicus.eu/cdsapp#!/dataset/10.24381/cds.adbb2d47?tab=overview (accessed on 7 April 2024).
21. Xin, L.; Hu, S.; Wang, F.; Xie, W.; Hu, D.; Dong, C. Using a deep-learning approach to infer and forecast the Indonesian Throughflow transport from sea surface height. *Front. Mar. Sci.* **2023**, *10*, 1079286. [CrossRef]
22. Akhil, V.P.; Lengaigne, M.; Durand, F.; Vialard, J.; Chaitanya, A.V.S.; Keerthi, M.G.; Gopalakrishna, V.V.; Boutin, J.; de Boyer Montégut, C. Assessment of seasonal and year-to-year surface salinity signals retrieved from SMOS and Aquarius missions in the Bay of Bengal. *Int. J. Remote Sens.* **2016**, *37*, 1089–1114. [CrossRef]
23. Ratna, S.B.; Cherchi, A.; Osborn, T.J.; Joshi, M.; Uppara, U. The Extreme Positive Indian Ocean Dipole of 2019 and Associated Indian Summer Monsoon Rainfall Response. *Geophys. Res. Lett.* **2021**, *48*, e2020GL091497. [CrossRef]
24. Ernst, P.A.; Subrahmanyam, B.; Trott, C.B. Lakshadweep High Propagation and Impacts on the Somali Current and Eddies During the Southwest Monsoon. *J. Geophys. Res. Ocean.* **2022**, *127*, e2021JC018089. [CrossRef]
25. Yuhong, Z.; Yan, D.; Shaojun, Z.; Yali, Y.; Xuhua, C. Impact of Indian Ocean Dipole on the salinity budget in the equatorial Indian Ocean. *J. Geophys. Res. Ocean.* **2013**, *118*, 4911–4923. [CrossRef]
26. Potemra, J.T.; Luther, M.E.; O'Brien, J.J. The seasonal circulation of the upper ocean in the Bay of Bengal. *J. Geophys. Res.* **1991**, *96*, 12667–12683. [CrossRef]
27. Suresh, I.; Vialard, J.; Lengaigne, M.; Izumo, T.; Parvathi, V.; Muraleedharan, P.M. Sea Level Interannual Variability Along the West Coast of India. *Geophys. Res. Lett.* **2018**, *45*, 12440–12448. [CrossRef]
28. Cheng, X.; McCreary, J.P.; Qiu, B.; Qi, Y.; Du, Y.; Chen, X. Dynamics of Eddy Generation in the Central Bay of Bengal. *J. Geophys. Res. Ocean.* **2018**, *123*, 6861–6875. [CrossRef]
29. Chen, G.; Han, W.; Li, Y.; McPhaden, M.J.; Chen, J.; Wang, W.; Wang, D. Strong Intraseasonal Variability of Meridional Currents near 5°N in the Eastern Indian Ocean: Characteristics and Causes. *J. Phys. Oceanogr.* **2017**, *47*, 979–998. [CrossRef]
30. Huang, H.; Wang, D.; Yang, L.; Huang, K. Enhanced Intraseasonal Variability of the Upper Layers in the Southern Bay of Bengal During the Summer 2016. *J. Geophys. Res. Ocean.* **2021**, *126*, e2021JC017459. [CrossRef]
31. Li, Z.; Long, Y.; Huang, S.; Xie, H.; Zhou, Y.; Yang, B.; Bai, Y.; Zhu, X.H. A Large Winter Chlorophyll-a Bloom in the Southeastern Bay of Bengal Associated With the Extreme Indian Ocean Dipole Event in 2019. *J. Geophys. Res. Ocean.* **2023**, *128*, e2022JC018791. [CrossRef]
32. Li, Y.; Han, W.; Ravichandran, M.; Wang, W.; Shinoda, T.; Lee, T. Bay of Bengal salinity stratification and Indian summer monsoon intraseasonal oscillation: 2. Impact on SST and convection. *J. Geophys. Res. Ocean.* **2017**, *122*, 4312–4328. [CrossRef]
33. McPhaden, M.J.; Foltz, G.R. Intraseasonal variations in the surface layer heat balance of the central equatorial Indian Ocean: The importance of zonal advection and vertical mixing. *Geophys. Res. Lett.* **2013**, *40*, 2737–2741. [CrossRef]
34. Han, W.; Li, Y.; Wang, W.; Ravichandran, M. Intraseasonal Variability of SST and Precipitation in the Arabian Sea during the Indian Summer Monsoon: Impact of Ocean Mixed Layer Depth. *J. Clim.* **2016**, *29*, 7889–7910. [CrossRef]
35. Ivanova, D.P.; McClean, J.L.; Sprintall, J.; Chen, R. The Oceanic Barrier Layer in the Eastern Indian Ocean as a Predictor for Rainfall Over Indonesia and Australia. *Geophys. Res. Lett.* **2021**, *48*, e2021GL094519. [CrossRef]
36. Rao, R.; Sivakumar, R. On the possible mechanisms of the evolution of a mini-warm pool during the pre-summer monsoon season and the genesis of onset vortex in the South-Eastern Arabian Sea. *Q. J. R. Meteorol. Soc.* **1999**, *125*, 787–809.